Engineered Science

RESEARCH PAPER

View Article Online

Stabilization and Metallic to Semiconducting Transition in 2D Boron Sheet

Zhifen Luo, Xiaoli Fan,* Yurong An, Yan Hu and Fengxia Zhang

Bucked triangular, β_{12} and χ_3 are the three lattices of atomic-thin boron sheet which have been realized experimental very recently. The three lattices all are metallic and dynamical unstable. By adopting the first-principles method based on the density functional theory, we predict the biaxial strain under which the β_{12} and χ_3 boron sheets are stabilized. We also demonstrate the effectiveness of hydrogenation on stabilize the buckled triangular boron sheet. Additional, our calculations show that neither uniaxial nor biaxial strain stabilizes the buckled triangular boron sheet, and when the applied biaxial strain is larger than 14%, its anisotropic conductivity no longer exists. Moreover, the electronic band structures of the three boron sheets are controllable by modifying the hydrogen coverage. We find the Dirac cone in the fully hydrogenated buckled triangular boron sheet, and the metal-semiconducting transition in β_{12} and χ_3 boron sheet caused by 100% and 50% hydrogenation. Our results reveal new electronic properties for the new class of 2D materials, borophene in the applications of electronics.

Keywords: Boron sheet; First-principles method; Hydrogen

Received 27th March 2018, Accepted 8th May 2018

DOI: 10.30919/es8d142

1. Introduction

Last two decade, atomic-thin boron sheets have attracted extensive attentions for exploring their atomic structures.[1–5] Recently, atomically thin 2D boron sheets have been synthesized on Ag(111) surfaces by the physical vapor deposition method.[1,2] These extended 2D boron sheet is called as 'borophene', in analogy to graphene. Three structures of borophene have been observed,[1,2] namely, buckled triangular, β_{12} and χ_3. The buckled triangular borophene is highly anisotropic metal with high Young's modulus along its armchair direction which exceeds that of graphene,[1] and its electronic and transport properties also strongly correlate with directions.[6] Additional, Gao et al predict the superconductivity of the β_{12} and χ_3 boron sheets.[7] Moreover, these three lattices of boron sheet all show potentials as an anode material for Li, Na and Mg ion batteries due to the high theoretical specific capacities and outstanding ion transport properties.[8–11]

With the advanced properties mentioned above, borophene definitely is the new promising 2D material in a vast applications field. According to the previous studies,[2,12–14] the formation energies of the three boron sheets of buckled triangular, β_{12} and χ_3 are very close. However, the phonon spectra for the buckled triangular, β_{12} and χ_3 borophene all show that these boron sheets are dynamically unstable,[1,14,15] which somehow limits their applications. Strain and surface functionalization have been proved to be effective on stabilizing the 2D materials.[15–20] Penev et al. proposed that the imaginary frequencies of both β_{12} and χ_3 borophene near the G point may be eliminated by applying a uniform tensile strain.[15] Additional, based on the first-principles calculations,[19,20] Xu et al. and Liu et al. predict that the fully hydrogenated buckled triangular borophene is dynamical stable without imaginary frequency.

Tunable band gap is one of the most desired properties in the application of 2D materials. Various methods have been developed to open the energy gaps of the 2D metallic materials, such as surface functionalization,[21–24] strain engineering[25–27] and electric field controlling[28,29] In this context, it is both necessary and important to investigate the effect of surface functionalization and strain on the electronic structures of buckled triangular, β_{12} and χ_3 boron sheets which all show metallic behavior.[1,2,7,14]

By performing the first principles calculations, we investigate the effect of strain and hydrogenation on the three boron sheets of buckled triangular, β_{12} and χ_3. Our calculations show that β_{12} and χ_3 boron sheets are dynamical stable under biaxial strain of 4.8% and 6.6%, respectively. But neither biaxial nor uniaxial strain can stabilize the free-standing buckled triangular borophene. Additional, all the three structures maintain metallic under the biaxial strain ranging from 0% to 10%. Moreover, we show that the adsorption of hydrogen turns the metallic β_{12} and χ_3 boron sheet into semiconducting with energy gaps of 1.1 and 0.8 eV.

2. Calculation details

Our calculations are performed by using the Vienna *ab-initio* simulation package (VASP) based on the density functional theory (DFT).[30,31] The projector-augmented-wave method was adopted for the calculations of electron-ion interactions.[32,33] And the electronic exchange–correlation

State Key Laboratory of Solidification Processing, Center for advanced lubrication and seal Materials, School of Material Science and Engineering, Northwestern Polytechnical University, 127 YouYi Western Road, Xi'an, Shaanxi 710072, China. E-mail: xlfan@nwpu.edu.cn

interactions were described by the generalized gradient approximation (GGA) by using the Perdew–Burke–Ernzerhof (PBE) function.[34] Wave functions were expanded in a plane wave basis with an energy cutoff of 500 eV. The 7×5×1, 5×3×1, 3×1×1 and 5×5×1 supercell were used to simulate the strained buckled triangular, β_{12}, χ_3 phases of borophene and hydrogenated χ_3 borophene, respectively. And their first Brillion zone were sampled by 25×15×1, 15×9×1, 15×5×1 and 11×11×1 k-mesh. To simulate the 2D boron sheets, a vacuum space of 20 Å is included along the Z direction to minimize the interaction between the periodic images. The convergence criterion was set to 10^{-8} eV between two ionic steps for the self-consistency calculations. All the atoms were fully relaxed until the force on each atom was less than 0.01 eV $Å^{-1}$. Phonon dispersion spectra have been computed by using the finite displacement method as implemented in the PHONOPY package.[35]

3. Results and discussion

3.1. Boron sheets under strain

Fig. 1 shows the atomic structures of the bucked triangular, β_{12} and χ_3 borophene. The buckled triangular boron sheet shows bucking along the lattice direction perpendicular to the B atoms plane. Our calculated lattice constants for the buckled triangular borophene are **a** = 1.613 Å and **b** = 2.866 Å, agreeing well with previous theoretical and experimental results.[1] As showing in Fig. 1(b) and (c), unlike the buckled triangular boron sheet, the β_{12} and χ_3 borophene are planar without out-of-plane buckling. The lattice constants for the β_{12} borophene are 2.916 Å and 5.075 Å along the **a** and **b** directions, respectively. The unit cell of β_{12} borophene is rectangle in which there are five B atoms. As for the χ_3 borophene, there are four B atoms in the rhombic unit cell, and the lattice constants are 4.448 Å.

We then studied the buckled triangular, β_{12} and χ_3 borophene under the uniaxial and biaxial strain ranging from -5% to 15%. As showing in Fig. 1, the rectangle unit cells are used to simulate the three lattices. The lattice constants for the rectangle unit cell of χ_3 borophene are **a** = 2.909 Å and **b** = 8.413 Å. Our calculations show that under the compressive strain, all the three lattices of buckled triangular, β_{12} and χ_3 become more unstable having larger imaginary frequencies, and the imaginary frequencies even increase as the compressive strain increases. Thus, we only report the results under the tensile strain in the present study.

Our calculations show that there are always imaginary frequencies in the phonon spectrum of buckled triangular borophene under both the uniaxial and biaxial strain up to 15%. It implies that neither biaxial nor uniaxial strain stabilizes the free-standing buckled triangular borophene. Fortunately, both the β_{12} and χ_3 phases of the boron sheets are stabilized under the biaxial stain. As showing in Fig. 2(a) and (b), there is no imaginary frequency in the phonon spectra for the β_{12} and χ_3 boron sheets under the biaxial stain of 4.8% and 6.6%. We also calculated the electronic band structures for the strained β_{12} and χ_3 borophene under the biaxial strain of 4.8% and 6.6%, respectively. It indicates that the stabilized β_{12} and χ_3 boron sheets remain metallic.

Figure 3 shows the electronic band structures for the strained buckled triangular, β_{12} and χ_3 borophene. As we can see, all the strained three lattices maintain to be metallic under the biaxial strain ranging from 0% to 15%. For all the three boron sheets under the increasing biaxial strain, their conduction bands move down and their valence bands shift up. Particularly, the buckled triangular borophene maintains to be metallic with strong anisotropy under the biaxial strain less than 14%, as showing in Fig. 3(a). Specifically, its electrical conductivity is confined along the uncorrugated **a** direction but it is semiconducting along the **b** direction. When the applied biaxial strain is larger 14%, the buckled triangular borophene loses the anisotropy, behaves metallic along all the lattice directions.

3.2. Boron sheets functionalized by hydrogen

We further studied the hydrogenated buckled triangular, β_{12} and χ_3 borophene at different hydrogen coverage. The calculation results are

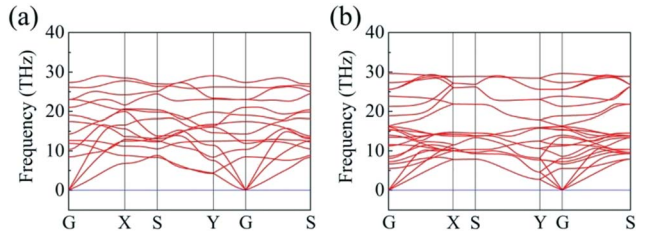

Fig. 2 The phonon spectra of the strained β_{12} and χ_3 boron sheets. (a) showing the data for β_{12} boron sheet under the biaxial stain of 4.8%; (b) showing the data for χ_3 boron sheet under the biaxial stain of 6.6%.

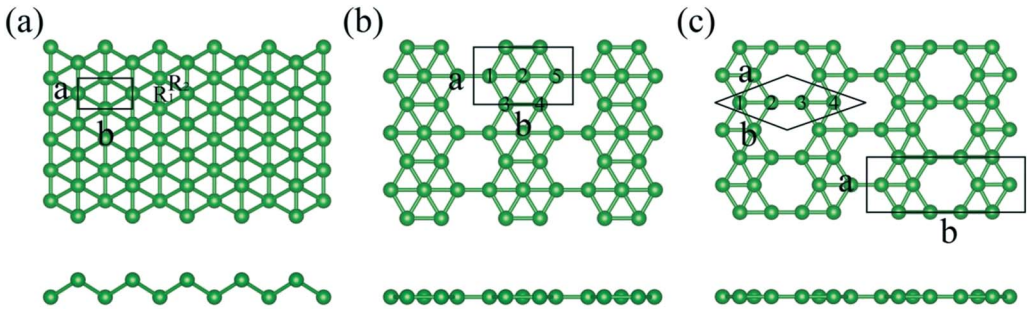

Fig. 1 Top and side views of (a) buckled triangular, (b) β_{12}, (c) χ_3 boron sheets. The green balls represent the boron atoms. The rectangles and rhombus enclosed by solid black lines denote the unit cells. The letters **a** and **b** represent the lattice parameters, R_1 and R_2 represent the two typical B-B bond. The numbers represent different boron atoms in the unit cell.

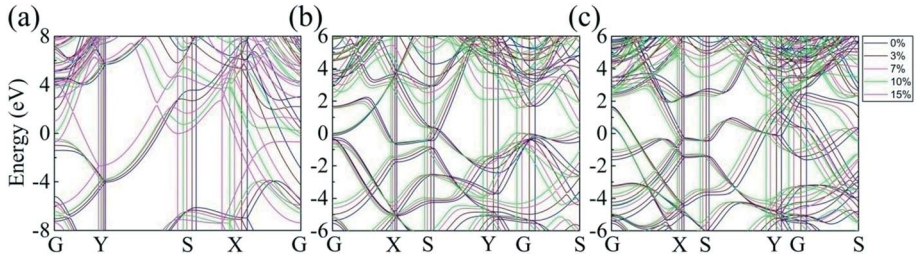

Fig. 3 The electronic band structures of (a) buckled triangular, (b) β_{12} and (c) χ_3 boron sheet under the biaxial strain ranging from 0% to 15%.

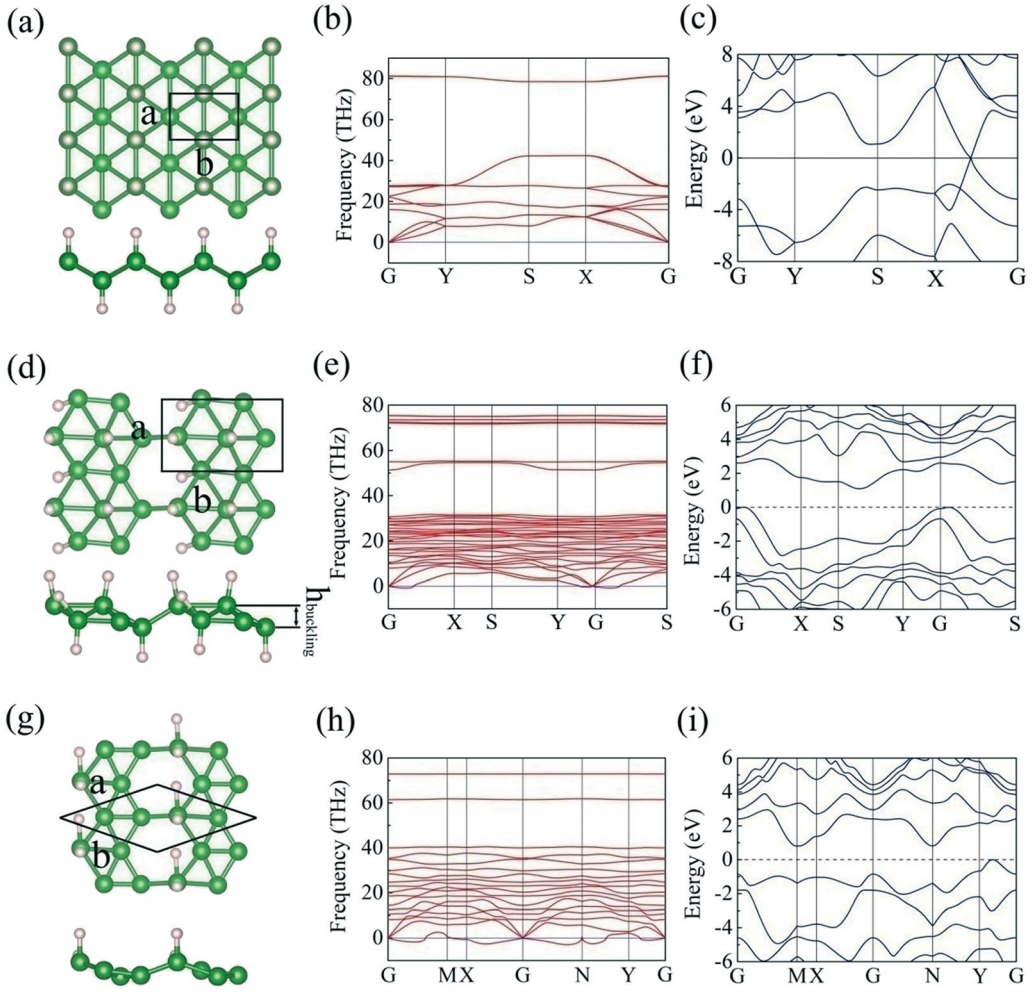

Fig. 4 The top and side view of the atomic structures, phonon spectra and electronic band structure of hydrogenated buckled triangular, β_{12} and χ_3 boron sheet. (a), (b) and (c) showing the data for the 100% hydrogenated buckled triangular boron sheet, (d), (e) and (f) showing the data for the 100% hydrogenated β_{12} boron sheet, (g), (h) and (i) showing the data for the 50% hydrogenated χ_3 boron sheet.

summarized in Table I-III. The adsorption energies of H atom adsorption on the boron sheet are calculated via

$$E_{ad} = (E_{tot} - E_{borophene} - \frac{n}{2} E_{H_2}) / n,$$

where E_{tot} and $E_{borophene}$ are the energies of the boron sheet with the adsorption of H atoms and the clean boron sheet; E_{H_2} and n are the energy of hydrogen molecule and the number of adsorbed H atoms, respectively.

Fig. 5(a) and 4(a) shows the atomic structures for the 50% and 100% hydrogenated buckled triangular boron sheets, respectively. In the 50% hydrogenated buckled triangular boron sheet, only the upper or lower B atoms are terminated by H atoms, and in the 100% hydrogenation case, both the upper and lower B atoms are hydrogenated. The 100% hydrogenated buckled triangular borophene is stabilized and there is no imaginary frequency in the phonon spectrum shown in Fig. 4(b), but the 50% hydrogenated buckled triangular borophene remains unstable. Our calculations tell us that the buckled triangular borophene can be

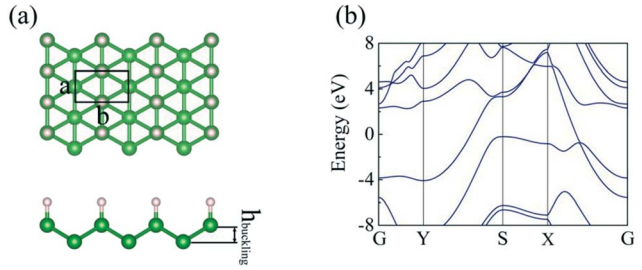

Fig. 5 The top and side view of the atomic structures and electronic band structures of 50% hydrogenated buckled triangular boron sheet.

stabilized by hydrogenation, which proves the previous result obtained by Xu et al.[19] Additional, as showing in Fig. 4(c), the calculated electronic band structure of fully hydrogenated buckled triangular borophene displays a clearly Dirac cone along X-G direction.

Unlike the buckled triangular boron sheet in which there are two B atoms in the unit cell and the two B atoms are symmetrically identical, there are five B atoms in the unit cell of β_{12} boron sheet and two pairs of B atoms are identical. They are labeled as "1" and "5" , and "3" and "4" as showing in Fig. 1(b). To study how the H atoms adsorb on the β_{12} boron sheet, we manually put H atom on three different B atom sites, "1", "2" and "3". Our calculations show that the adsorption energy of hydrogen on site "1", "2" and "3" atoms sites are -0.247 eV, 0.958 eV and -0.002 eV, respectively. This means that H atom prefers to adsorb on the "1" B atom site. Fig. 6(a) shows the atomic structure for the hydrogenated β_{12} boron sheet at 20% coverage in which one H atom adsorb on the "1" B atom site in each unit cell.

The hydrogenated β_{12} boron sheet at high H coverage were examined by adding H atoms at the less favorable B atom sites one by one. Fig. 6 show the lowest energy configurations for the hydrogenated β_{12} boron sheet at 20%, 40%, 60%, and 80% coverage. Our calculations indicate that the β_{12} borophene remains unstable under all kinds of hydrogenation structures. Fig. 6 shows the electronic band structures along the high symmetry directions for the 20%, 40%, 60% and 80% hydrogenated β_{12} borophene which maintain to be metallic, but the energy bands near the Fermi level become sparse. However, there is no energy band crossing the Fermi level for the 100% hydrogenated β_{12} borophene as showing in Fig. 4(f). It indicates that the fully hydrogenated β_{12} borophene is semiconducting, and its energy gap is 1.1 eV.

The hydrogenated χ_3 borophene was studied in the similar way as we studied the hydrogenated β_{12} boron sheet. There are four different B atoms in the unit cell of χ_3 borophene as showing in Fig. 1(c), and Fig. 7 shows our results for the most stable configurations of the hydrogenated χ_3 borophene at 25%, 50%, 75% and 100% coverage. Our calculations show that the surface functionlization by H atom fails to stabilize the χ_3 borophene. There are always negative values in the phonon spectra of the hydrogenated χ_3 boron sheet, and the imaginary frequencies even become bigger with the increasing of H coverage. Although hydrogenation turns out to be ineffective on stabilizing the χ_3 borophene, but it makes the χ_3 borophene convert from metal into semiconductor. The electronic band structure shown in Fig. 4(i) indicates that the 50% hydrogenated χ_3 borophene is semiconducting with energy gap of 0.8 eV.

Tables 1-3 summarize our calculation results with the lowest energies for the hydrogenated buckled triangular, β_{12} and χ_3 boron sheets at all

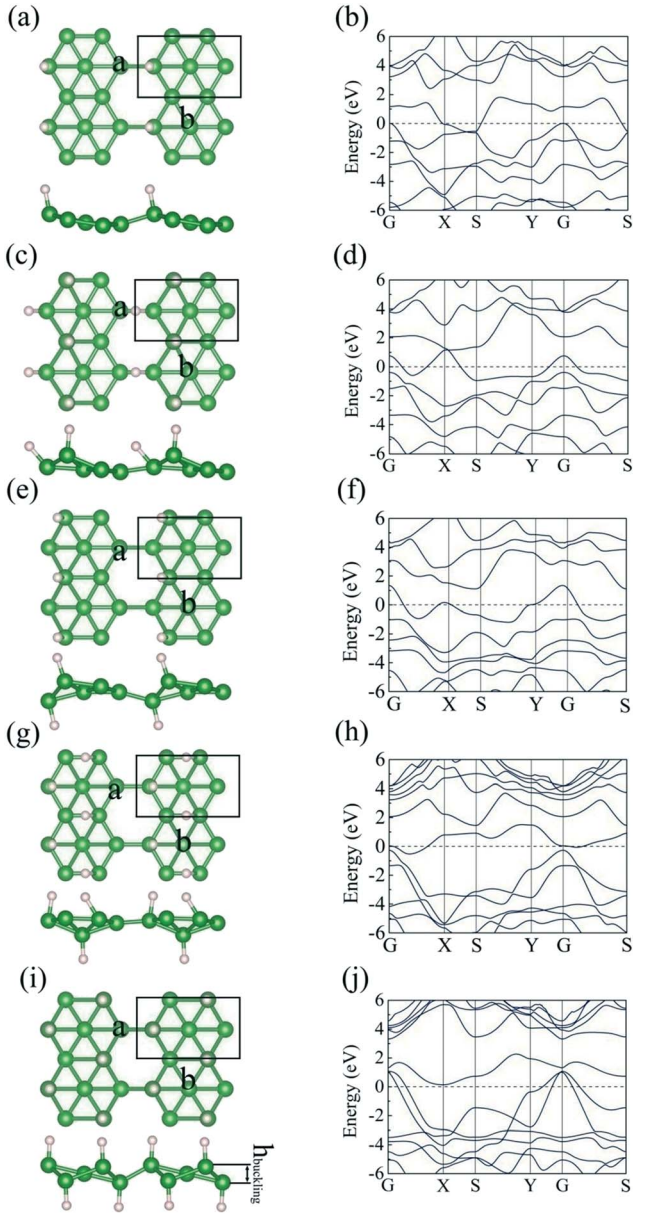

Fig. 6 The top and side view of the atomic structures and electronic band structures of 20%, 40%, 60%, and 80% hydrogenated β_{12} boron sheet. (a) and (b) showing the data for the 20% hydrogenated β_{12} boron sheet; (c) and (d) showing the data for the 40% hydrogenated β_{12} boron sheet; (e) and (f) showing the data for the 40% hydrogenated β_{12} boron sheet with hydrogen adsorption on the two sides; (g) and (h) showing the data for the 60% hydrogenated β_{12} boron sheet; (i) and (j) showing the data for the 80% hydrogenated β_{12} boron sheet.

the possible H coverage. We can see that the lattice constants and B-B bond lengths for the three boron sheets with the adsorption of H atoms at various H coverage are almost as same as those of the bare boron sheets except for the 100% hydrogenated buckled triangular boron sheet. For the 100% hydrogenated buckled triangular boron sheet, the **a** lattice constant and the B-B bond length along the **a** direction increase by 0.3 Å, while the **b** lattice constant and the B-B bond along the **b** direction hardly change. Additional, the buckling height of the buckled triangular boron sheet decreases after the adsorption of H. Nevertheless, the β_{12} and χ_3 boron sheets are not planar any more with

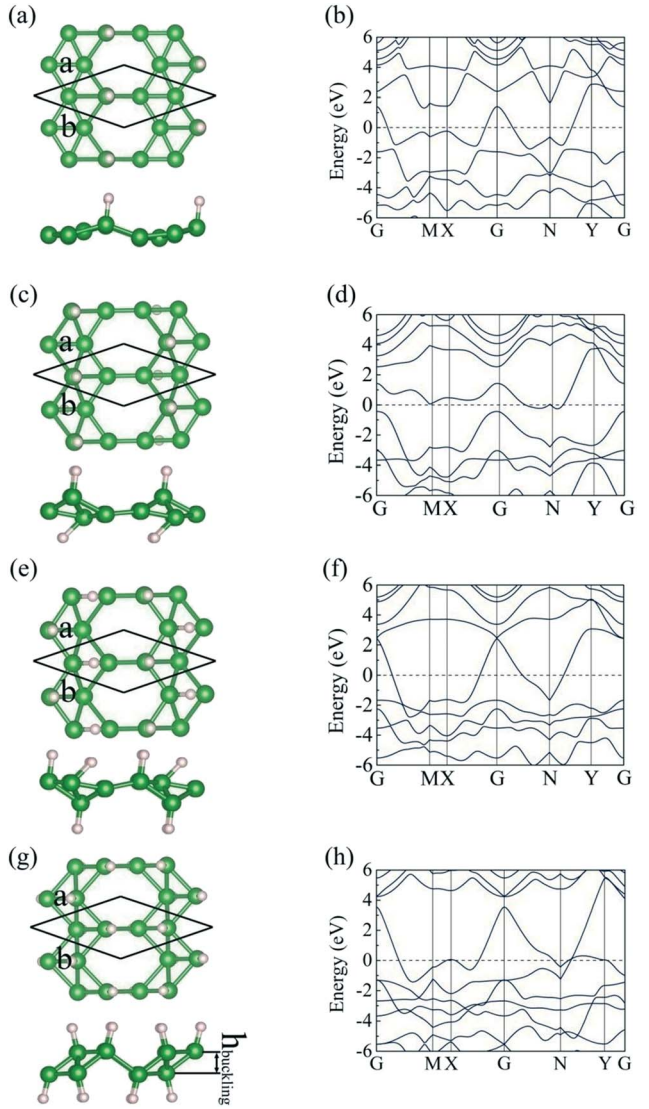

Fig. 7 The top and side view of the atomic structures and electronic band structures of 25%, 50%, 75% and 100% hydrogenated χ_3 boron sheet. (a) and (b) showing the data for the 25% hydrogenated χ_3 boron sheet; (c) and (d) showing the data for the 50% hydrogenated χ_3 boron sheet with hydrogen adsorption on the two sides; (e) and (f) showing the data for the 75% hydrogenated χ_3 boron sheet; (g) and (h) showing the data for the 100% hydrogenated χ_3 boron sheet.

the adsorption of H as showing in Fig. 6 and 7, and the buckling heights increase by 0.9-1.0 Å at most with the increasing of H coverage. Despite the buckling appearing along the vertical direction as a result of interaction between the H atoms and B atoms, the in-plane configurations maintain to be as same as the bare boron sheet. In Table 1-3, the adsorption energies are calculated via $E_{ad} = (E_{tot} - E_{borophene} - \frac{n}{2}E_{H_2})/n$, which actually is the averaged formation energy of several B-H bonds. Under high hydrogen coverage for one side adsorption, the adsorption energies are positive, which means that the B-H bond become weak. Hence, we put hydrogen on both sides to increase hydrogen coverage. For the double side

Table 1 The calculation results on the buckled triangular borophene and hydrogenated buckled triangular borophene. **a** and **b** represent the lattice constants. $h_{buckling}$ is the vertical distance between the upper and lower boron atoms. R_1 and R_2 represent the typical B-B bond lengths which are showing in Fig. 1. d_{B-H} is the bond length between boron atoms and the bonded hydrogen atoms. E_{ad} is the adsorption energy of hydrogen on the boron sheet.

	a(Å)	b(Å)	$h_{buckling}$(Å)	R_1(Å)	R_2(Å)	d_{B-H}(Å)	E_{ad} (eV)
$b_\triangle$	1.613	2.866	0.910	1.613	1.879	/	/
$b_\triangle$-50%H	1.613	2.866	0.875	1.613	1.863	1.211	0.468
$b_\triangle$-100%H	1.938	2.825	0.803	1.941	1.888	1.180	-0.163

Table 2 The calculation results on the β_{12} borophene and hydrogenated β_{12} borophene. **a** and **b** represent the lattice constants. $h_{buckling}$ is the vertical distance between the upper and lower boron atoms. d_{B-H} is the bond length between boron atoms and the bonded hydrogen atoms. E_{ad} is the adsorption energy of hydrogen on the boron sheet.

	a(Å)	b(Å)	$h_{buckling}$(Å)	d_{B-H}(Å)	E_{ad} (eV)
β_{12}	2.916	5.075	0	/	/
β_{12}-20%H	2.916	5.057	0.582	1.227	-0.247
β_{12}-40%H	2.908	5.042	0.888	1.219	0.333
β_{12}-40%H#	2.911	5.047	0.956	1.214	-0.138
β_{12}-60%H	2.906	5.040	0.817	1.249	-0.218
β_{12}-80%H	2.863	5.018	0.847	1.212	-0.168
β_{12}-100%H	2.927	5.075	0.904	1.232	-0.157

result of 40% hydrogenated β_{12} boron sheet with hydrogen adsorption on the two sides.

hydrogen adsorption, the adsorb energy would be first decreases and then increases as the H atoms coverage becoming higher. Consequently, the most stable configurations of the functionalized boron sheets are 100% hydrogenated buckled triangular, 20% hydrogenated β_{12} and 75% hydrogenated χ_3 boron sheets.

4. Conclusions

By performing the density functional theory type of first-principles calculations, we studied the atomic structures, stability and electronic property of the strained and hydrogenated atomic-thin boron sheets. We find that the β_{12} and χ_3 boron sheets are stabilized under the biaxial stain of 4.8% and 6.6%. But, there are always imaginary frequencies for the buckled triangular borophene under the biaxial strain up to 15%. When the biaxial is larger than 14%, the buckled triangular borophene loses the anisotropic metallic character. Additional, our calculations show that hydrogenation is effective on stabilizing the buckled triangular borophene, but neither β_{12} nor χ_3 borophene are stabilized under kinds of hydrogenation coverages. Moreover, we find that the fully hydrogenated β_{12} and 50% hydrogenated χ_3 borophene transit into semiconducting. Our calculations not only find the possible way to stabilize the three most important lattices of atomic-thin boron sheets, also highlight the new electronic property for the atomic-thin boron sheets.

Conflicts of interest

There are no conflicts to declare.

Table 3 The calculation results on the χ_3 borophene and hydrogenated χ_3 borophene. **a, b** and **γ** represent the lattice constants. $h_{buckling}$ is the vertical distance between the upper and lower boron atoms. $d_{B\text{-}H}$ is the bond length between boron atoms and the bonded hydrogen atoms. E_{ad} is the adsorption energy of hydrogen on the boron sheet.

	a(Å)	b(Å)	γ	$h_{buckling}$(Å)	$d_{B\text{-}H}$(Å)	E_{ad} (eV)
χ_3	4.448	4.448	38.182°	0	/	/
χ_3-25%H	4.427	4.427	38.182°	0.530	1.221	-0.061
χ_3-50%H	4.449	4.449	38.182°	0.617	1.257	0.247
χ_3-50%H$^{\#}$	4.418	4.418	38.182°	0.936	1.272	-0.311
χ_3-75%H	4.412	4.412	38.182°	0.926	1.248	-0.352
χ_3-100%H	4.384	4.384	38.182°	1.119	1.194	-0.060

result of 50% hydrogenated χ_3 boron sheet with hydrogen adsorption on the two sides.

Acknowledgments

This work was supported by the 111 Project (B08040), the Fundamental Research Funds for the Central Universities (3102015BJ(II)JGZ005, 3102015BJ023) in China and National Natural Science Foundation of China(21273172). The supports from the University of Science and Technology Beijing and the University of Electronic Science and Technology China are appreciated.

References

1 A. J. Mannix, X. F. Zhou, B. Kiraly, J. D. Wood, D. Alducin, B. D. Myers, X. Liu, B. L. Fisher, U. Santiago, J. R. Guest, M. J. Yacaman, A. Ponce, A. R. Oganov, M. C. Hersam and N. P. Guisinger, *Science*, 2015, **350**, 1513–1516.
2 B. J. Feng, J. Zhang, Q. Zhong, W. B. Li, S. Li, H. Li, P. Cheng, S. Meng, L. Chen and K. H. Wu, *Nat. Chem.*, 2016, **8**, 563–568.
3 C. Romanescu, D. J. Harding, A. Fielicke and L. S. Wang, *J. Chem. Phys.*, 2012, **137**, 5803.
4 W. An, S. Bulusu, Y. Gao and X. C. Zeng, *J. Chem. Phys.*, 2006, **124**, 154310.
5 P. Tandy, M. Yu, C. Leahy, C. S. Jayanthi and S. Y. Wu, *J. Chem. Phys.*, 2015, **142**, 124106.
6 J. E. Padilha, R. H. Miwa and A. Fazzio, *Phys. Chem. Chem. Phy.*, 2016, **18**, 25491.
7 M. Gao, Q. Z. Li, X. W. Yan and J. Wang, *Phys. Rev. B*, 2017, **95**, 024505.
8 X. M. Zhang, J. P. Hu, Y. C. Cheng, H. Y. Yang, Y. G. Yao and S. Y. A. Yang, *Nanoscale*, 2016, **8**, 15340.
9 H. R. Jiang, Z. H. Lu, M. C. Wu, F. Ciucci and T. S. Zhao, *Nano Energy*, 2016, **23**, 97–104.
10 Y. Zhang, Z. F. Wu, P. F. Gao, S. L. Zhang and Y. H. Wen, *ACS Appl. Mater. Inter.*, 2016, **8**, 22175.
11 B. Mortazavi, A. Dianat, O. Rahaman, G. Cuniberti and T. Rabczuk, *J. Power Sources*, 2016, **329**, 456–461.
12 T.X. Wu, J. Dai and Y. Zhao, *ACS Nano*, 2012, **6**, 7443.
13 F. Ma, Y. Jiao and G. Gao, *Nano Lett.*, 2016, **16**, 3022–3028.
14 Z. F. Luo, X. L. Fan and Y. R. An, *Nanoscale Res. Lett.*, 2017, **12**, 514.
15 E. S. Penev, A. Kutana and B. I. Yakobson, *Nano Lett.*, 2016, **16**, 2522.
16 C. W. Zhang and S. S. Yan, *J. Phys. Chem. C*, 2016, **116**, 4163–4166.
17 Y. Wang and Y. Ding, *J. Mater. Chem. C*, 2016, **4**, 7485–7493.
18 B. Wang, J. Wu, X. Gu, H. Yin, Y. Wei, R. Yang and M. Dresselhaus, *Appl. Phys. Lett.*, 2014, **104**, 081902.
19 L. C. Xu, A. J. Du and L. Z. Kou, *Phys. Chem. Chem. Phy.*, 2016, **18**, 27284.
20 G. Liu, H. Wang, Y. Gao, J. Zhou and H. Wang, *Phys. Chem. Chem. Phy.*, 2017, **19**, 2843–2849.
21 X. Xin, W. Li, R. Pang, H. Wang, C. Guo, X. Shi and Y. Zhao, *Appl. Phys. Lett.*, 2017, **111**, 253102.
22 X. Zhang, X. Zhao, D. Wu, Y. Jing and Z. Zhou, *Nanoscale*, 2015, **7**, 16020–16025.
23 M. Khazaei, M. Arai, T. Sasaki, C. Y. Chung, N. S. Venkataramanan, M. Estili, Y. Sakka and Y. Kawazoe, *Adv. Funct. Mater.*, 2013, **23**, 2185–2192.
24 L. Sun, Q. Li, H. Ren, H. Su and J. Yang, *J. Chem. Phys.*, 2008, **129**, 074704.
25 E. Scalise, M. Houssa, G. Pourtois, V. Afanas'ev and A. Stesmans, *Nano Res.*, 2012, **5**, 43–48.
26 A. S. Rodin, A. Carvalho and A. H. Castro Neto, *Phys. Rev. Lett.*, 2014, **112**, 176801.
27 F. Guinea, M. I. Katsnelson and A. K. Geim, *Nat. Phys.*, 2010, **6**, 30–33.
28 Y. ZhangT. T. Tang, C. Girit, Z. Hao, M. C. Martin, A. Zettl, M. F. Crommie, Y. R. Shen and F. Wang, *Nature*, 2009, **459**, 820–823.
29 T. Cao, Z. Li and S. G. Louie, *Phys. Rev. Lett.*, 2015, **114**, 236602.
30 G. Kresse and J. Furthmuller, *Phys. Rev. B: Condens. Matter*, 1996, **54**, 11169–11186.
31 G. Kresse and J. Furthmuller, *Comp. Mater. Sci.*, 1996, **6**, 15–50.
32 G. Kresse and D. Joubert, *Phys. Rev. B: Condens. Matter*, 1999, **59**, 1758–1775.
33 P. E. Blöchl, *Phys. Rev. B: Condens. Matter*, 1994, **50**, 17953–17979.
34 J. P. Perdew, K. Burke and M. Ernzerhof, *Phys. Rev. Lett.*, 1996, **77**, 3865–3868.
35 A. Togo and I. Tanaka, *Scripta Mater.*, 2015, **108**, 1–5.